Renewable Energy 226 (2024) 120467

Contents lists available at ScienceDirect

Renewable Energy

journal homepage: www.elsevier.com/locate/renene

Understanding platinum-based H2 adsorption/ desorption kinetics during catalytic hydrogenation or hydrogen storage-related reactions

Aleksandra Zamljen [a,b], Žan Lavrič [a], Anže Prašnikar [a], Janvit Teržan [a], Miha Grilc [a], Anton Meden [b], Blaž Likozar [a,*]

[a] Department for Catalysis and Chemical Reaction Engineering, National Institute of Chemistry, Hajdrihova 19, 1001 Ljubljana, Slovenia
[b] Faculty of Chemistry and Chemical Technology, University of Ljubljana, Večna pot 113, 1001 Ljubljana, Slovenia

ARTICLE INFO

Keywords:
Platinum catalyst
Hydrogen
Nanoparticle size
Temperature programmed desorption
Kinetic modelling

ABSTRACT

Hydrogen is among the most promising energy carriers and plays an important role on the way to sustainable technologies. Platinum holds great promise for unlocking the potential of renewable hydrogen, as it is an essential component of proton exchange membrane technologies and in various hydrogenation reactions. For the variety of applications of energy harvesting, conversion, and storage, the optimization and reduction of Pt loading is crucial. In view of this, a platinum catalyst using a stable SiO_2 support is synthesized to investigate the adsorption/desorption behavior of hydrogen on platinum nanoparticles of different sizes, obtained by treating the sample at different calcination temperatures. Pulsed chemisorption and subsequent temperature-programmed desorption are described mathematically to obtain kinetic parameters. It is shown that higher adsorption capacities could be obtained using smaller particles. However, for particles smaller than 2.4 nm, higher Pt^{2+} content decreases H_2 adsorption. Adsorption inhibition due to the presence of monatomic Pt cannot be excluded. The size of the Pt nanoparticles does not significantly affect the desorption/adsorption energy, but there is evidence that the hydrogen adsorbed per Pt atom at the surface varies with size: about 1 for single crystal planes and 2 for nanoparticles <3 nm.

1. Introduction

In recent decades, energy demand has increased rapidly. Although the use of fossil resources is declining, they are still an important source of energy, making the use of renewable energy sources essential to meet the ever-increasing demand for energy. One of the most prominent technologies among the alternatives is hydrogen technology, which can contribute significantly to carbon neutrality. Hydrogen is not only the most abundant and simplest element in the universe, but also has the highest energy content among existing energy sources and is therefore considered a sustainable fuel. Moreover, its oxidation product consists only of water, so it does not pollute the atmosphere [1,2].

Due to its unique chemical and physical properties, platinum plays an important role in the hydrogen industry as it is a key element in proton exchange membrane (PEM) technology. PEMs are used both in electrolysis for hydrogen production as well as in hydrogen fuel cells, the latter also being used to power electric vehicles, due to their low operating temperature and high efficiency [3–6]. In PEM fuel cells platinum nanoparticles are used as the most effective catalyst currently available for both the oxidation of hydrogen at the anode and the reduction of oxygen at the cathode [3]. Both gasses are adsorbed and dissociated into atoms, so one of the important parameters is also the activation energy barrier of adsorption (Ea_{ads}) and the activation energy of desorption (Ea_{des}) of a gas molecule on the catalyst. Reactants must adsorb strongly enough to atomize, but also be able to desorb and not block the active sites of the catalyst. Catalysts that bind hydrogen too weakly are limited by hydrogen adsorption, while catalysts that bind hydrogen too strongly are limited by hydrogen desorption [7]. Among all metals, Pt has the best-known properties for the described phenomenon. In general, catalysts are supported on carriers to ensure homogeneous distribution of the catalyst [3,7,8]. Here, adsorption in the gas phase was determined. Since solvation has a great influence on adsorption in electrolysis, other investigations should be carried out for this purpose. Platinum catalysts are widely used in industrial processes

* Corresponding author.
E-mail addresses: aleksandra.zamljen@ki.si (A. Zamljen), zan.lavric@ki.si (Ž. Lavrič), anze.prasnikar@ki.si (A. Prašnikar), janvit.terzan@ki.si (J. Teržan), miha.grilc@ki.si (M. Grilc), anton.meden@fkkt.uni-lj.si (A. Meden), blaz.likozar@ki.si (B. Likozar).

https://doi.org/10.1016/j.renene.2024.120467
Received 6 December 2023; Received in revised form 29 February 2024; Accepted 7 April 2024
Available online 8 April 2024

and in scientific research, especially for hydrogenations, hydrodeoxygenations, and/or decarbonylations [9]. Moreover, the sustainable and environmentally friendly production of hydrogen is an essential component of green energy. Currently, 96 % of the world's hydrogen is still produced from fossil resources [4]. The most promising method for green hydrogen production is water electrolysis powered by electricity from renewable energy sources [10]. High purity hydrogen needed for storage and subsequent electricity generation can be produced using PEM electrolyzers. Most electrolyzers contain PEM and thus platinum as an integral component [4,11]. Carbon-based Pt materials are used for HER (hydrogen evolution reaction) because Pt gives excellent HER activity and stability in acidic environment [12,13].

One of the biggest challenges in the transition to a hydrogen economy and thus in shaping a sustainable society is also the efficient and safe storage of hydrogen. Currently established storage technologies, such as pressurized liquid or gas storage, require heavy cylinders and/or extremely low temperatures and therefore pose a safety risk [14]. In recent years, research has focused on solid hydrogen storage materials such as complex metal hydrides (e.g., $LiBH_4$) [15] and metal-organic frameworks (MOFs) [14]. Additional doping of the latter with rare metals, particularly platinum or palladium, is expected to improve the material's ability to store hydrogen at ambient temperature. For example, UiO 66 (Zr-terephthalate MOF) [16] doped with platinum nanoparticles, Pt@ZIF-8/GO [17], and Pt-doped IRMOF-8 [18] have shown improved hydrogen storage capacity due to hydrogen spillover compared to undoped materials at room temperature. The kinetics of hydrogen adsorption and desorption is a crucial parameter for comparing different materials and their suitability for hydrogen storage [14,16–19].

When hydrogen molecules are adsorbed on the surface of a platinum catalyst, a dissociative chemisorption process takes place. Hydrogen is molecularly chemisorbed onto platinum so that the antibonding σ* orbital of the hydrogen molecule is filled by electrons from the platinum surface. After chemisorption, the hydrogen molecules dissociate on the platinum surface [20]. Unfortunately, Pt-based catalysts are expensive, so efforts have been made to reduce the Pt loading or to find an alternative to Pt-based electrocatalysts [21–23]. The amount of Pt used can be reduced by proper use – it is important to understand the influence of nanoparticle structure and size [23,24], as the findings could be extended to other metals to optimize environmentally relevant reactions such as methanol and ammonia synthesis. It was observed that Au single-atom catalysts can be efficiently used for the CO PrOx reaction (CO preferential oxidation) in the presence of O_2 and H_2. With clustering of Au atoms, the selectivity for this reaction decreased, leading to parasitic H_2 oxidation [25]. The size effect of the catalytic properties of Pt nanoparticles was studied for quinoline hydrogenation, and a drastic decrease in activity was observed when the size of Pt NP was decreased to 0.7 nm [26]. However, to the best of our knowledge, there are no data on H_2 adsorption capacity and detailed kinetics measured at different Pt particle sizes.

The focus of this study was to synthesise the platinum catalyst with different NP (nanoparticle) sizes on a SiO_2 support and to mathematically describe the adsorption and desorption of hydrogen on platinum to better understand the underlying process and to compare the obtained parameters between the materials. Extensive characterizations were performed to understand the structure and chemistry of material, including X-ray diffraction (XRD), transmission electron microscopy (TEM), X-ray photoelectron spectroscopy (XPS), scanning electron microscopy with energy dispersive spectroscopy (SEM-EDS), and inductively coupled plasma optical emission spectroscopy (ICP-OES). Pulsed chemisorption followed by temperature programmed desorption (TPD) was performed on each sample. To characterise the adsorption and desorption behaviour, the data from TPD were then further analysed using kinetic modelling, determining the kinetics of adsorption and desorption. A quantitative structural/mechanistic understanding of the adsorption/desorption of H_2 onto/from Pt, while critical to a variety of energy harvesting, conversion, and storage processes, has not been fully consolidated or understood to date.

2. Results and discussion

2.1. Structural characterization

All XRD powder patterns of the reduced catalyst (Pt/SiO_2) show a broad diffraction peak at 22° 2θ, indicating the amorphous nature of the SiO_2 support (Fig. 1) like previously observed in the literature [26]. The XRD powder patterns of catalyst calcined at 100 °C and 200 °C do not show characteristic diffraction peaks for Pt, indicating the absence of a significant number of Pt particles above ~5 nm previously identified under similar conditions (Pt loading, SiO_2 support) [26]. The linear dimension of NP is so small that it contains only a few unit cells. Consequently, they show amorphous nature. As expected [26], calcination leads to coarsening of the Pt, resulting in an increase in Pt-based signals when the temperature is raised above 400 °C. Generally, the positions of the Pt peaks agree well with the values of the standard pattern of Pt (PDF No. 00-004-0802), as the representative diffraction peaks for the face-centered cubic (fcc) Pt crystallites were observed at 39.7° (111), 46.3° (200), 67.4° (220), and 81.2° (311). Furthermore, the (111), (200), (220) planes of Pt were used to calculate the average crystallite sizes (d_{XRD}) using the Scherrer equation. The average crystallite size of the samples calcined at 600 °C and 400 °C is about 15 nm and 6 nm, respectively.

As can be seen in Fig. 2, as the calcination temperature increases, aggregation of the Pt-NP occurs, with the red arrows showing particles and the yellow arrows showing aggregates. It can be seen that the average particle size increases at higher calcination temperatures. In addition, the histograms of Pt particle size distribution were obtained by measuring the sizes of 150 randomly selected particles from each of the corresponding TEM images (Fig. 3). The Gaussian function was used to fit the experimental data. The average Pt particle sizes (d_{TEM}) for catalyst calcined at 100 °C, 200 °C, 400 °C, and 600 °C are (1.3 ± 0.5) nm, (2.4 ± 0.8) nm, (3.0 ± 0.9) nm, and (3.4 ± 1.0) nm, respectively. Catalyst calcined at 400 °C, and 600 °C also contain large particles (up to 16 nm). Compared to the smaller particles, their occurrence is lower and their contribution to the Pt surface area is therefore small. Hence, the values obtained from TEM analysis are more relevant than the values obtained from XRD analysis. As can be seen from the TEM images, the Pt NPs are only up to a few nm in size, therefore the samples calcined at 100 °C and 200 °C do not show representative Pt diffraction peaks. As

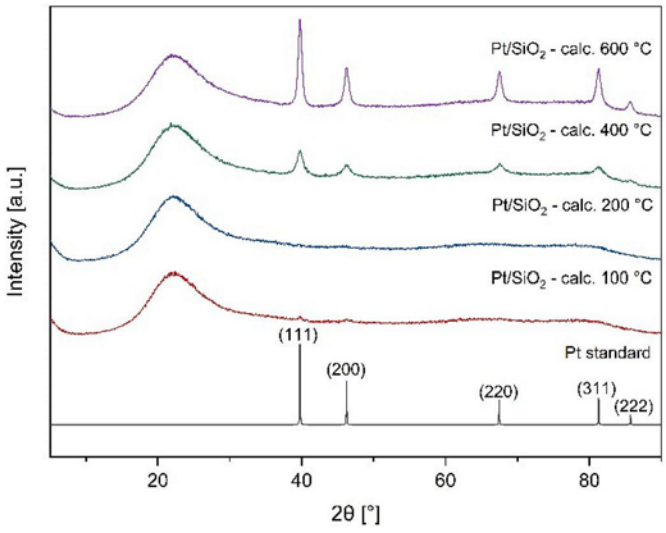

Fig. 1. XRD patterns of the Pt standard and Pt/SiO_2 catalyst, calcined at different temperatures.

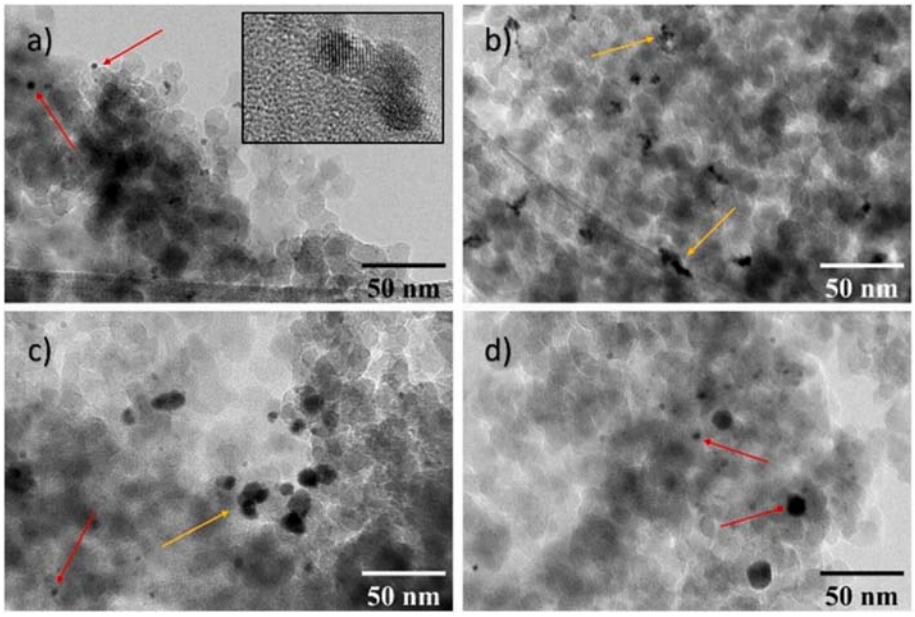

Fig. 2. TEM images of Pt/SiO_2 catalyst, calcined at different temperatures: a) 100 °C and Pt interplanar spacing, b) 200 °C, c) 400 °C, d) 600 °C and then reduced in H_2 at 250 °C.

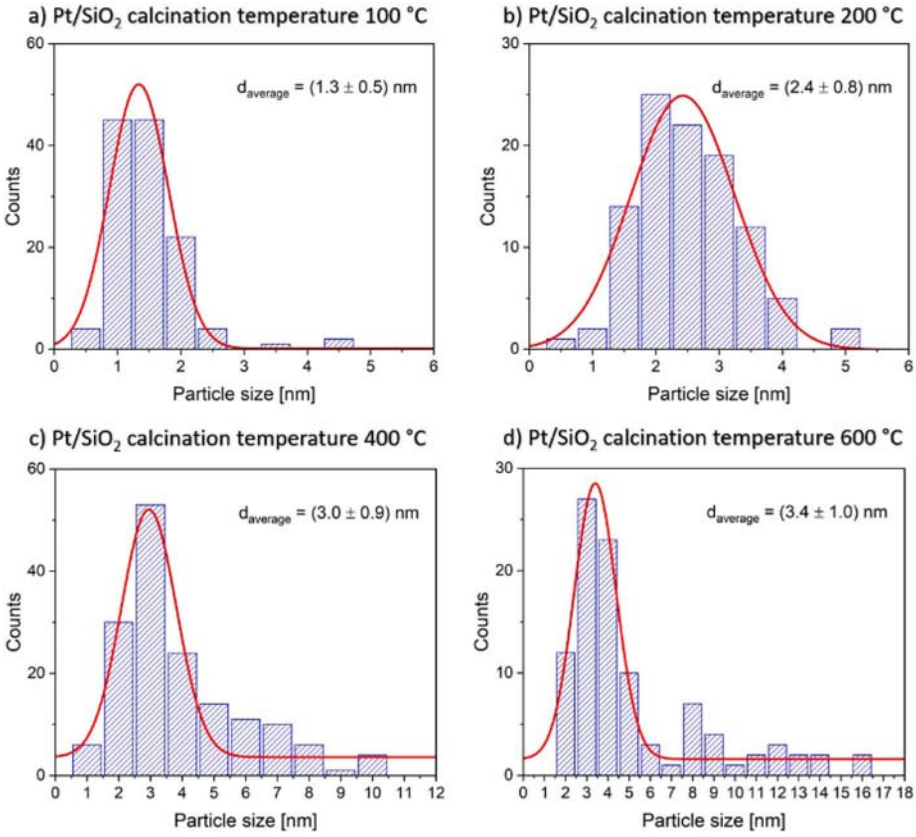

Fig. 3. Pt nanoparticle size distribution and Gaussian fit for different calcination temperatures.

can be seen from interplanar spacing (measured $d = 2.353$ Å) of Pt in Fig. 2a, the Pt nanoparticle belongs to the (111) crystal plane.

From the ICP-OES analysis the actual Pt content in Pt/SiO_2 was estimated to be 1.31 wt%, which is close to the expected Pt loading of 1.38 wt% from the synthesis. The EDS elemental mapping of the catalyst calcined at 600 °C was performed to verify the homogeneity of the sample (Fig. S2). Fig. 4 shows the part of the sample on which the EDS analysis was performed and a uniform spatial distribution of silicon (Si), oxygen (O) and platinum (Pt) elements, indicating a uniform distribution of Pt NPs on the surface of the SiO_2 support. Conductive carbon tape was used for the EDS analysis therefore, carbon was also detected.

H_2 pulsed adsorption (H_2 PA) followed by temperature programmed-

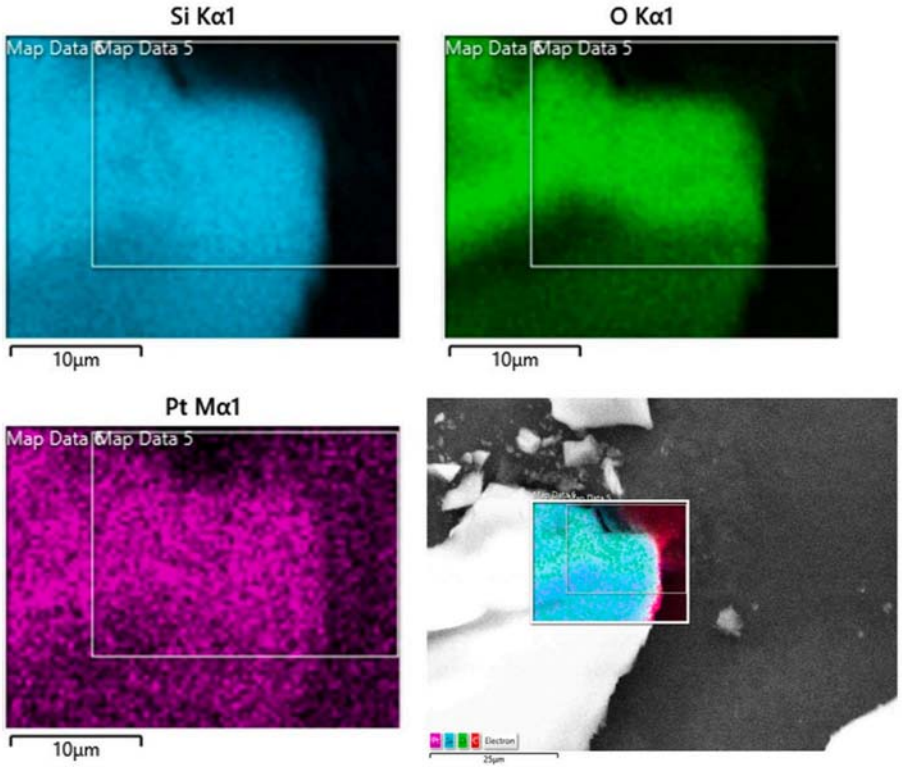

Fig. 4. A part of the sample on which SEM analysis was performed and EDS elemental mapping of three elements (Si, O, Pt) of the sample calcined at 600 °C.

desorption (H_2 TPD) was used to determine the kinetics of H_2 adsorption and desorption on the synthesized catalyst. The repeatability of the measurements was confirmed (Fig. S3) with a relative error of approximately 3 % (Table S1). The H_2 consumption per mass of sample varied significantly for catalyst, treated at different calcination temperatures. Fig. 5 shows pulsed chemisorption and TPD analyzes for the catalyst (Pt/SiO_2) calcined at different temperatures. Three consecutive pulsed chemisorption and TPD measurements were performed for each sample. In the first measurement, the largest amount of H_2 was adsorbed. A slight decrease in adsorption was observed in the second and third cycles, due to incomplete desorption between successive cycles (Fig. S4). Fig. 8 shows the average amount of hydrogen adsorbed with an absolute error. Normalized to the mass of the sample, the highest H_2 adsorption is observed for the catalyst synthesized at a calcination temperature of 200 °C. As expected, the lowest adsorption is observed for the sample calcined at 600 °C (see Fig. 5).

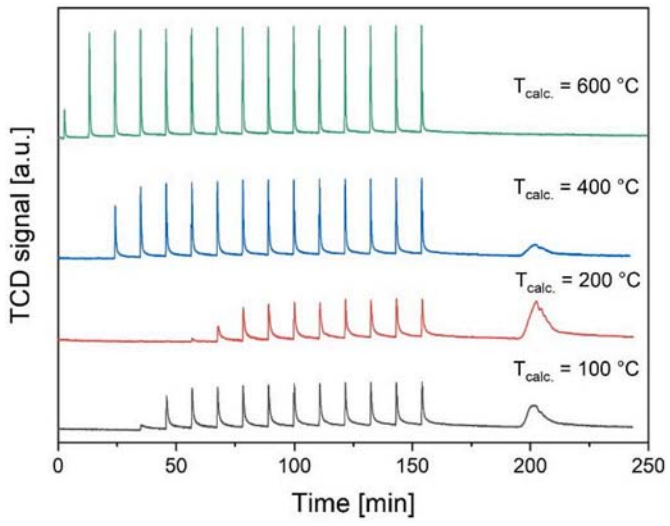

Fig. 5. Comparison of pulsed chemisorption and TPD measurements for a catalyst calcined at different temperatures.

The size of the Pt nanoparticles has a significant effect on the amount of H_2 adsorbed. As shown in the TEM analyses, the use of different calcination temperatures before reduction results in Pt nanoparticles of different sizes. As the size of the nanoparticles decreases, the ratio of surface to bulk atoms increases, making more surface atoms available for the reaction. Nevertheless, the catalytic performance is not always directly proportional to the increased surface area of the nanoparticles [27]. Here, a volcano shaped dependence of the catalytic activity on the size of the Pt nanoparticles was observed. Nanoparticles of (2.4 ± 0.8) nm exhibited the highest activity in the adsorption of hydrogen.

No desorption peak was observed for the catalyst calcined at 600 °C, although some amount of H_2 was adsorbed. The signal does not return to baseline immediately after the adsorption step, therefore the desorption peak is hidden in the baseline. The latter can be clearly seen when comparing the TPD signal with the kinetic model.

XPS analysis revealed the presence of two platinum species in the materials at lower reduction temperatures (Fig. 6). The corresponding binding energies of 71.2 and 72.4 eV for the first two peaks can be attributed to Pt^0 and Pt^{2+}, respectively [28]. We believe that the Pt^{2+} species is the lowest layer of Pt nanoparticles bound to the support via the Pt–*O*–Si oxygen bridges, as shown by Pt–O instead of Pt–Pt in the EXAFS of 1.2 nm Pt on SiO_2 [26]. As a remainder, oxidized Pt is observed here even though it was exposed to 1 bar of H_2 at 250 °C for 2 h. When the temperature is increased during thermal treatment, the relative intensity of the peak at 72.4 eV gradually decreases. We assume that this is a very good indication of particle growth. The larger the particles, the smaller the relative amount of Pt atoms that form these oxygen bridges. Very small particles, such as those produced by heat treatment at 100 °C, have a high relative amount of Pt–O that may not bind H_2 (Fig. 9).There are at least two reasons for this. Oxidation of Pt reduces H–Pt bonding, and the other reason is that a fraction of Pt is in the form of single Pt

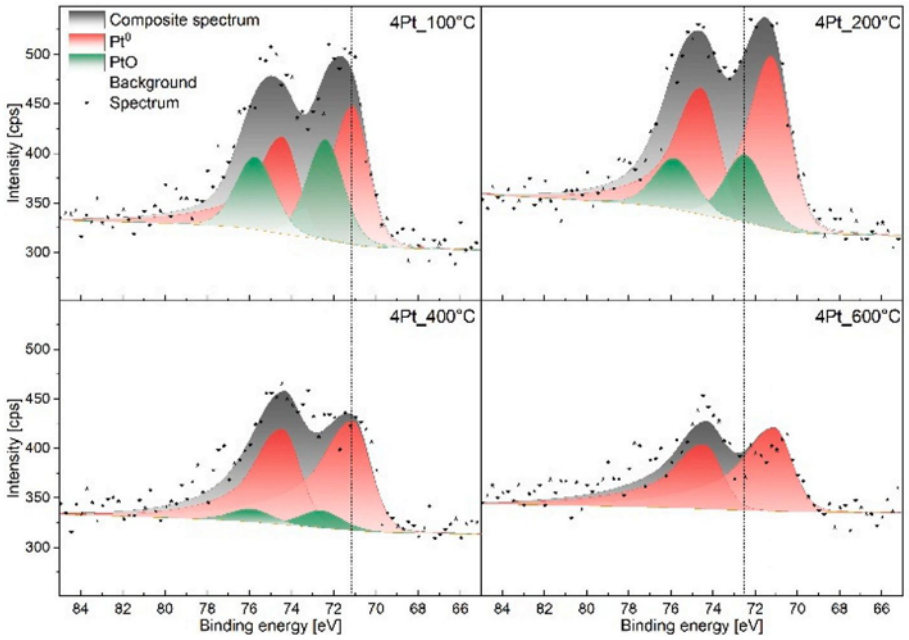

Fig. 6. XPS analysis of a catalyst calcined at different temperatures.

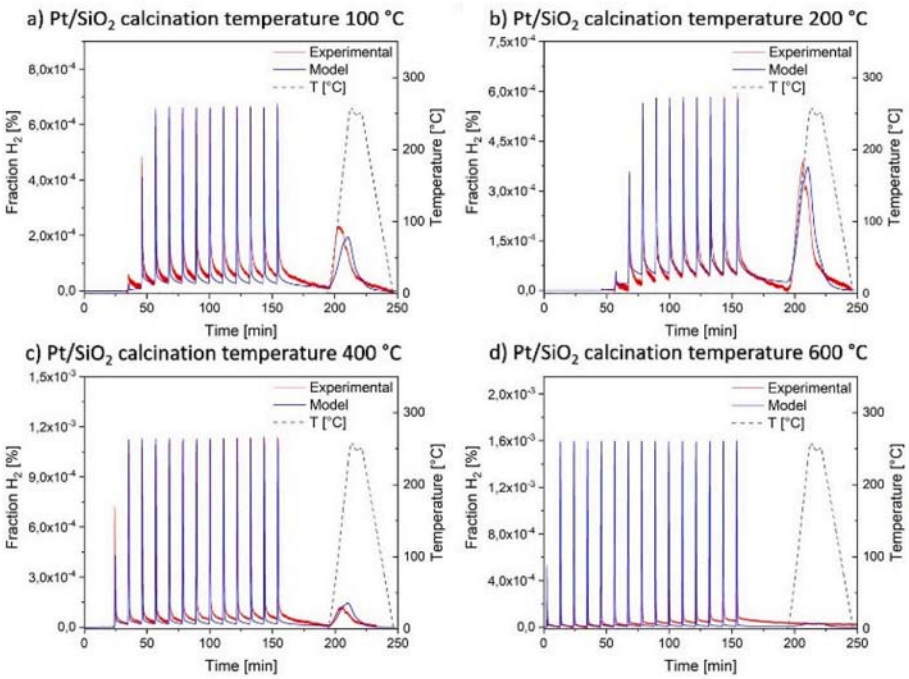

Fig. 7. Comparison of pulsed chemisorption and TPD for samples, calcined at different temperatures.

atoms. Similar to Au [25], Pt single atoms might be able to adsorb and cleave H_2 molecules. Density functional theory calculations have shown that the type of Pt atom support coordination determines the Gibbs free energy of H–Pt, which varies between −0.26 eV and 0.57 eV (H at Pt (111) equals −0.17 eV) [29]. At first glance, replacement of oxidic support with carbonaceous one could decrease the amount of Pt–O bonds and possibly increase H_2 adsorption. However, EXAFS results show Pt–O in the Pt single atom/graphene sample even after reduction in 0.2 bar H_2 at 200 °C [29], demonstrating a strong environmental impact on reactive Pt at high dispersion. In contrast, larger particles, such as those formed at 400 °C and above, have a lower relative proportion of surface Pt atoms that bind H_2. To substantiate this quantitatively, we plotted H/Pt_{tot} as a function of XPS Pt/Si ratio and found that there is a rough correlation between metallic Pt and adsorbed hydrogen (Fig. S5). The optimal temperature, balancing Pt dispersion and the oxidation state/structure, for treating the materials presented is therefore 200 °C yielding uniform Pt NPs with the average size of 2.4 nm.

Another possible explanation is that the particles are so small that they have a low ratio of ensembles, which are crucial for adsorption. In the field of catalysis, a promising hypothesis is derived from ensemble theory. According to this hypothesis the availability of specific ensembles of surface atoms influences reactivity. As the size of the particle decreases, the ratio of these ensembles changes. Since certain metal sites

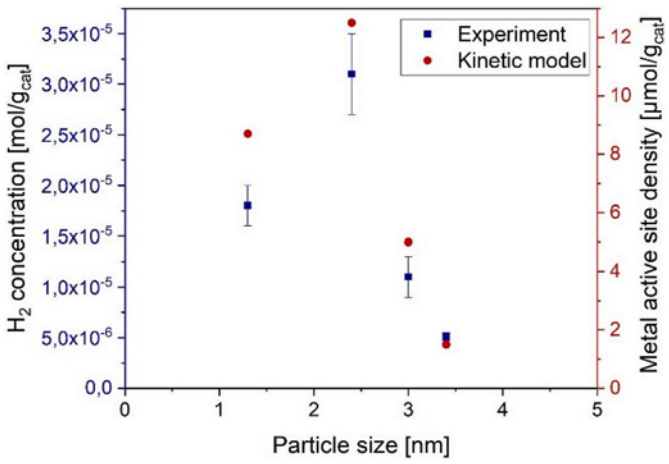

Fig. 8. Comparison of adsorbed concentration of H_2 with metal active sites density, obtained from kinetic model.

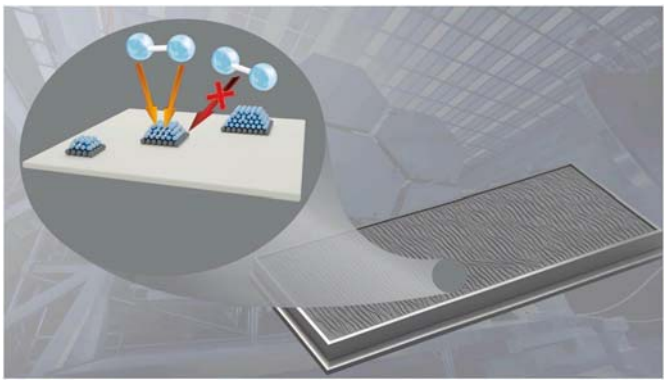

Fig. 9. H_2 molecules dissociatively adsorb on Pt^0, but cannot adsorb on PtO as oxidation of Pt reduces Pt–H bonding.

are believed to be primarily responsible for the reactivity of a metal nanoparticle, the decreased proportion of the latter may lead to decreased reactivity, in this case hydrogen adsorption [30,31]. Bai et al. also observed a volcano shaped dependence of the catalytic activity on the size of the Pt NPs for the hydrogenation of quinoline [26].

2.2. Calculation of dispersion and Pt nanoparticle size from TPD measurement

Selective chemisorption is commonly used for the characterization of metal catalysts. Quantitative measurement of the adsorbed gas on the metal, assuming the formation of a monolayer, enables the dispersion to be calculated when the stoichiometry of the chemisorption reaction is known. Generally, H_2 adsorbs dissociatively on platinum with a stoichiometry of one hydrogen atom per metal atom (H/Pt_{surf}) [32,33]:

$$H_2 + 2\ Pt \rightarrow 2\ Pt\text{–}H$$

Once the amount of gas chemisorbed/desorbed on a monolayer has been determined (n_{ads}), the metal surface area can be determined. The metal surface area can then be conventionally expressed in terms of the metal weight in the catalyst:

$$A_{met} = \frac{N_A \bullet n_{ads} \bullet F_S \bullet a_{met}}{X_{met}} \quad 1$$

where N_A is the Avogadro constant, F_S is the stoichiometric factor, a_{met} is the square section of a metal atom (8.07 Å^2) [34], and X_{met} is the percentage of metal (wt%, determined by ICP OES). The metal dispersion, defined as the ratio between the number of adsorbing metal atoms and the total number of metal ions in the catalyst, was calculated using the following equation:

$$\frac{H}{P_{t_{tot}}} = D_{met} = \frac{n_{ads} \bullet F_S \bullet M_{met}}{X_{met}} \quad 2$$

where M_{met} represents the molecular weight of Pt. In addition, the average size of the metal aggregates was also calculated as follows:

$$d_{met} = \frac{S_f}{A_{met} \bullet \rho_{met}} \quad 3$$

Assuming that Pt NPs are spherical, the S_f factor is equal to 6, while ρ_{met} represents the metal density [35].

As can be seen from Table 1, the measured particle sizes differ significantly among different methods. From TEM images it can be seen that larger nanoparticles form at calcination temperatures of 400 °C and 600 °C (up to 16 nm), but their abundance is quite low compared to smaller nanoparticles. The latter is also the reason for the significant difference in particle size determined by XRD and TEM mentioned above. Relatively small particles, only up to a few nanometers in size, contain only a few unit cells in the linear dimension. Consequently, the peaks in XRD are so broad that they are hidden in the background and only the diffraction peaks of larger particles are visible in the diffraction pattern. In general, all methods show that the nanoparticles have a larger size at higher calcination temperatures. The highest value for H/Pt_{tot} (or dispersion) calculated from TPD experiments, was also obtained for a calcination temperature of 200 °C. At 100 °C, the calculated dispersion is much lower than the literature value reported by Miller et al. (0.95) at the same calcination temperature, which is explained above by the structure and/or Pt oxidation state. The measured H/Pt_{tot} at calcination temperatures of 200 °C, 400 °C, and 600 °C, are in better agreement with the literature data. The reported H/Pt_{tot} at 400 °C and 600 °C were 0.47 and 0.11, respectively, while H/Pt of the sample calcined at 200 °C should be between 0.8 and 0.9, which is similar to the measured value [36].

A single value for H/Pt_{surf} stoichiometry has a limited use. The typical H/Pt_{surf} stoichiometry on Pt(111) was reported to be around 1 [33], and in the case of >3 nm sized Pt NPs similar CO/Pt_{tot} and H/Pt_{tot} have been observed [32]. However, recent calculations show that for small clusters [37] or single Pt atoms [38] the H/Pt_{surf} ratio can reach or even exceed a value of 2. Based on the size and shape of the observed NPs with TEM, we estimated the dispersions and found that the measured H/Pt is about 2 times higher than the estimated dispersion using TEM data in the case of the sample calcined at 200 °C, while for the other samples other parameters could affect the correlation, such as the oxidation state of Pt at low calcination temperature or strong agglomeration at high calcination temperature. By combining all the data, we present here an experimental evidence of the actual H/Pt_{surf} values.

Table 1
Pt NP size, dispersion and Pt/Si atomic surface ratio obtained with different techniques and dispersion.

*T*calcination [°C]	H/Pt [/]	*d*met [nm]	*d*TEM [nm]	*d*XRD [nm]	*DTEM* [/]	*Pt/Si XPS [0.001]*
100 °C	0.55	2.02	1.3 ± 0.5	/	0.86	4.24
200 °C	0.93	1.20	2.4 ± 0.8	/	0.47	4.17
400 °C	0.36	3.14	3.0 ± 0.9	6	0.37	3.25
600 °C	0.08	13.84	3.4 ± 1.0	15	0.33	1.85

2.3. Kinetic modelling of pulsed chemisorption and temperature programmed desorption

The kinetic model describes both the concentration of the gas phase and the coverage of the active sites of the catalyst throughout the fixed-bed reactor (in this case, the reactor is a quartz tube) as a function of time. Catalytic activity was investigated in the dynamic regime as a function of the catalyst layer length and time. Axial convection of the gas through the void space in the catalytic bed, axial diffusion in the gas phase, adsorption, and desorption kinetics were considered in the model.

In each time interval or axial coordinate increment, the adsorption rate (r_{ads}) for the given adsorbate (j) is influenced by the adsorption rate constant (k_j^{ads}) [39], the concentration of the adsorbate in the gas phase (C_j), and a fraction of the vacant active sites (θ_{AS}) (**Equation (4)**). However, the desorption rate (r_j^{des}) depends only on the desorption rate constant (k_j^{des}) and the surface coverage of compound j (**Equation (5)**):

$$r_j^{ads} = k_j^{ads} \bullet C_j \bullet \theta_{AS} \quad 4$$

$$r_j^{des} = k_j^{des} \bullet \theta_j \quad 5$$

The model includes balances for both gas concentrations and surface cover to predict kinetic parameters. The differential equations for the gas concentrations (C_j) consist of the contribution of convective flux and adsorption and desorption rates, while diffusive and radial flux were neglected (**Equations 6 and 7**). v_z, V_G and n_{AS} represent the linear velocity of the gas in the axial direction (x), the volume of the void in the bed, and the total amount of available active surface sites, respectively. The calculation of set parameters if explained further in the supporting information **(Equation S1 to S5)**.

$$\frac{\partial C_j}{\partial t} = -\frac{\partial}{\partial z}\left[v_z \bullet C_j\right] - r_j^{ads} + r_j^{des}\frac{n_{TS}}{V^G} \quad 6$$

$$\frac{\partial \theta_j}{\partial t} = r_j^{ads}\frac{V^G}{n_{TS}} - r_j^{des} \quad 7$$

Pulsed chemisorption and TPD data were used as input data to determine the adsorption and desorption rates (r_{ads} and r_{des}), and the corresponding activation energies *Ea*. As mentioned earlier, the adsorption and desorption rates, activation energy, and number of active sites were used as input data for the regression analysis. The calcination of the catalyst particles at different temperatures affects the number of metallic active sites, available for H_2 adsorption. Fig. 7 shows the experimental (red line) and modelled (blue line) data from four experiments at the fixed-bed outlet.

Unlike other techniques for estimating desorption activation energy, such as Redhead analysis, leading edge analysis, or others, full finite difference modelling of the system allows us to consider every parameter, resulting in data with higher accuracy and fewer assumptions. The rate constants for adsorption and desorption at 0 °C are 717 ± 13 min^{-1} and 14.1 ± 0.5 min^{-1}, respectively, which is consistent with the data where H_2 introduced at the entrance of the fixed bed is adsorbed at all available active sites. Once there are no more available adsorption sites, the H_2 molecules pass through the catalyst bed. However, since the peaks are not symmetrical, either some desorption occurs even when the temperature of the bed is 0 °C, or H_2 is adsorbed onto the tube material or other surface that occurs upstream of the TCD sensor. When TPD is initiated, temperature affects the adsorption/desorption rate constant ratio, and H_2 is desorbed from the surface. The activation energies of the adsorption and desorption reactions are 16 ± 1 and 41 ± 3 kJ mol^{-1}, respectively. Because the activation energy of desorption is two times higher, the value of the desorption rate constant exceeds the value of the adsorption rate constant, minutes after heating, and H_2 gas is desorbed from the material.

The kinetic model describes the experimentally determined values relatively well, although the adsorption reaction involves both adsorption of the H_2 molecule and dissociation to atoms. Since dissociation proceeds much faster than molecular adsorption, dissociation was neglected, and *Ea* of adsorption is actually a pseudo constant that includes both. The literature reports on *Ea* of desorption for similar material are relatively scarce. Christman et al. [33] calculated the activation energy of desorption for H_2 from Pt(111) surface to be 39.7 kJ mol^{-1}, which coincides with our calculation.

3. Conclusion

Through paramount to a plethora of energy harvesting, conversion, and storage processes, the quantitative structural/mechanistic understanding of H_2 adsorption/desorption onto/from Pt has not been consolidated or grasped to date. The effect of Pt nanoparticle size on the H_2 adsorption and desorption behavior of hydrogen on an irreducible SiO_2 support was investigated. Different sizes of Pt nanoparticles were obtained using the strong electrostatic adsorption method and different calcination temperatures, while keeping the noble metal loading constant, which increased the consistency and accuracy of the observed trends. According to the analytical procedures, the Pt nanoparticles were homogeneously distributed on the support. As expected, higher calcination temperatures resulted in larger particles. The larger the particles, the smaller the fraction of surface atoms, leaving fewer atoms available for adsorption of hydrogen. However, when the particles are smaller than 2.4 nm, an increasingly higher fraction of Pt^{2+} is observed, leading to a decrease in the H_2 adsorption capacity, although a possible adsorption inhibition due to the presence of single atom Pt cannot be neglected. The results showed that the catalyst calcined at 200 °C contained the largest number of active sites. Pulsed chemisorption and temperature-programmed desorption were analysed using kinetic modelling. The model indicates that the size of the Pt nanoparticles has no significant effect on the activation energy of desorption or adsorption, although the amount of hydrogen per surface Pt atom could vary with particle size, being about 1 for exposed single crystal planes and 2 for nanoparticles around and below 3 nm. To further improve the study, materials doped with Pt could be investigated in terms of the hydrogen adsorption kinetics, in which the spillover effect is present, so as to address the limitations of the hydrogen storage. Moreover, Pt materials have a great potential as catalysts in catalytic dehydrogenation process in liquid organic hydrogen carriers technology.

4. Experimental section

Synthesis of Pt/SiO2 catalyst: Synthesis of 1.4 wt% Pt on silica was carried out by strong electrostatic adsorption (SEA). 5 g of silica (Silica Aerosil 200V, Degussa AG) was slurried in 44.5 mL H2O (18 MΩ). The pH was raised to 9.8 by addition of concentrated NH4OH (Fluka). Then, 0.14 g of $Pt(NH_3)_4(NO_3)_2$ (Aldrich), previously dissolved in 7.7 mL of H_2O, was added. After 1 h, the product was transferred to a conical centrifuge tube and centrifuged. The solid was washed with 2 x 10 mL H_2O and dried overnight at 100 °C in flowing air. Pt elemental analysis determined by using ICP-OES (inductively coupled plasma optical emission spectrometer) gave 1.31 wt%. The Pt/SiO_2 catalyst was calcined in flowing air at 100 °C, 200 °C, 400 °C, and 600 °C by heating at 1 °Cmin^{-1} until the final temperature was reached and then held for 3 h. After calcination, the samples were reduced at atmospheric pressure in flowing H_2 (140 mLmin^{-1}) by heating from room temperature at 5 °Cmin^{-1} to 250 °C and holding for 2 h.

Characterization of Pt/SiO2 catalyst: Energy dispersive spectroscopy was performed on a scanning electron microscope (SEM, SUPRA35 VP, Carl Zeiss) coupled with an EDS detector (Inca 400, Oxford Instruments). The sample was pelletized and placed on the carbon tape previously attached to a on metal support. Analyses were performed on five sites of the sample calcined at 600 °C at 20 kV and an aperture size of 120 μm for 1 min. Inductively coupled plasma optical emission

spectrometry using a Varian 715 ES ICP Optical Emission Spectrometer was used to determine Pt loading. X-ray diffraction analyses were performed using a PANalytical X'Pert Pro MPD instrument with Bragg-Brentano geometry and Cu Kα1 radiation source. XRD patterns were acquired in a range of 5°–90° 2θ, with a measurement increment of 0.05° and a step time of 1000 s. The size of Pt nanoparticles was determined using transmission electron microscopy (TEM, JEM-2100, Jeol Inc.) operating at an accelerating voltage of 200 kV and equipped with a CCD camera. The images were analysed using ImageJ. X-ray photoelectron spectroscopy (XPS) was performed with the PHI VersaProbe 3 AD (Phi, Chanhassen, US), which uses a monochromatic Al Kα X-ray source. For charge neutralisation, the charge of the sample was attenuated using two beams (electrons and ions). The peak shift caused by neutralisation was corrected to 284.8 eV by shifting the peaks of the adventitious carbon species. The survey spectra were measured at a transit energy of 224 eV with a step of 0.8 eV. The high-resolution spectra were measured at a transit energy of 27 eV with a step of 0.05 eV. For the survey spectra, 2 sweeps were performed, while for the high-resolution spectra, 20 sweeps were performed. Spectral deconvolution was performed using Multipak software.

Adsorption experiments: Pulse chemisorption and temperature-programmed desorption analyses were performed to quantify the amount of hydrogen adsorbed/desorbed and consequently evaluate the number of H_2 adsorption sites. Approximately 150 mg of the powdered samples were placed in a U-shaped quartz reactor on a quartz wool (Micromeritics Autochem 2920 apparatus). The H_2 concentration was monitored using TCD (thermal conductivity detector), while the absence of impurities was determined using a mass spectrometer (Pfeiffer ThermoStar GSD 301 T3 Benchtop). 5 vol% H_2 in Ar (Messer, 5.0) was used for the experiments. Further information is provided in the Supporting information (Fig. S1).

CRediT authorship contribution statement

Aleksandra Zamljen: Conceptualization, Data curation, Formal analysis, Investigation, Methodology, Writing – original draft, Writing – review & editing. **Žan Lavrič:** Data curation, Validation, Writing – original draft. **Anže Prašnikar:** Conceptualization, Formal analysis, Supervision, Validation, Writing – original draft, Writing – review & editing. **Janvit Teržan:** Formal analysis, Writing – original draft. **Miha Grilc:** Investigation, Supervision. **Anton Meden:** Conceptualization, Supervision. **Blaž Likozar:** Conceptualization, Funding acquisition, Supervision, Writing – review & editing.

Declaration of competing interest

The authors declare that they have no known competing financial interests or personal relationships that could have appeared to influence the work reported in this paper.

Acknowledgements

This work was funded by the Slovenian Research and Innovation Agency through Programme P2-0152 and the research projects N2-0291, N2-0310, J2-4441, J2-4433, J1-3028, N1-0196, and J7-4638. Edi Kranjc is acknowledged for XRD measurement and Dr. Sašo Gyergyek for TEM measurement. We would also like to thank Alen Rupnik for his contribution to the graphical abstract.

Appendix A. Supplementary data

Supplementary data to this article can be found online at https://doi.org/10.1016/j.renene.2024.120467.

References

[1] J. Liu, S. Japip, T.-S. Chung, Hydrogen storage in molecular clathrate cages under conditions of moderate pressure and ambient temperature, Int. J. Hydrog. Energy 43 (2018) 19998–20003, https://doi.org/10.1016/j.ijhydene.2018.09.044.
[2] M. Kaur, K. Pal, Review on hydrogen storage materials and methods from an electrochemical viewpoint, J. Energy Storage 23 (2019) 234–249, https://doi.org/10.1016/j.est.2019.03.020.
[3] O.T. Holton, J.W. Stevenson, The role of platinum in proton exchange membrane fuel cells, Platin, Met. Rev. 57 (2013) 259–271, https://doi.org/10.1595/147106713X671222.
[4] S. Shiva Kumar, V. Himabindu, Hydrogen production by PEM water electrolysis – a review, Mater. Sci. Energy Technol. 2 (2019) 442–454, https://doi.org/10.1016/j.mset.2019.03.002.
[5] M. İnci, Connecting multiple vehicular PEM fuel cells to electrical power grid as alternative energy sources: a Case Study, Int. J. Hydrog. Energy 52 (2024) 1035–1051, https://doi.org/10.1016/j.ijhydene.2023.08.228.
[6] M. Büyük, M. İnci, Improved drift-free P& O MPPT method to enhance energy harvesting capability for dynamic operating conditions of fuel cells, Energy 267 (2023) 126543, https://doi.org/10.1016/j.energy.2022.126543.
[7] I.T. McCrum, M.T.M. Koper, The role of adsorbed hydroxide in hydrogen evolution reaction kinetics on modified platinum, Nat. Energy 5 (2020) 891–899, https://doi.org/10.1038/s41560-020-00710-8.
[8] Y. Devrim, E.D. Arıca, Multi-walled carbon nanotubes decorated by platinum catalyst for high temperature PEM fuel cell, Int. J. Hydrog. Energy 44 (2019) 18951–18966, https://doi.org/10.1016/j.ijhydene.2019.01.051.
[9] R. Šivec, M. Huš, B. Likozar, M. Grilc, Furfural hydrogenation over Cu, Ni, Pd, Pt, Re, Rh and Ru catalysts: Ab initio modelling of adsorption, desorption and reaction micro-kinetics, Chem. Eng. J. 436 (2022) 135070, https://doi.org/10.1016/j.cej.2022.135070.
[10] L. Yang, R. Grzeschik, P. Jiang, L. Yu, C. Hu, A. Du, S. Schlücker, W. Xie, Tuning the electronic properties of platinum in hybrid-nanoparticle assemblies for use in hydrogen evolution reaction, Angew. Chem. Int. Ed. 62 (2023), https://doi.org/10.1002/anie.202301065.
[11] S.A. Grigoriev, A.A. Kalinnikov, Mathematical modeling and experimental study of the performance of PEM water electrolysis cell with different loadings of platinum metals in electrocatalytic layers, Int. J. Hydrog. Energy 42 (2017) 1590–1597, https://doi.org/10.1016/j.ijhydene.2016.09.058.
[12] W. Xu, K. Scott, The effects of ionomer content on PEM water electrolyser membrane electrode assembly performance, Int. J. Hydrog. Energy 35 (2010) 12029–12037, https://doi.org/10.1016/j.ijhydene.2010.08.055.
[13] Y. Lei, Y. Wang, Y. Liu, C. Song, Q. Li, D. Wang, Y. Li, Designing atomic active centers for hydrogen evolution electrocatalysts, Angew. Chem. Int. Ed. 59 (2020) 20794–20812, https://doi.org/10.1002/anie.201914647.
[14] H.W. Langmi, J. Ren, B. North, M. Mathe, D. Bessarabov, Hydrogen storage in metal-organic frameworks: a review, Electrochim. Acta 128 (2014) 368–392, https://doi.org/10.1016/j.electacta.2013.10.190.
[15] Z. Ding, S. Li, Y. Zhou, Z. Chen, W. Yang, W. Ma, L. Shaw, LiBH4 for hydrogen storage - new perspectives, Nano. Mater. Sci. 2 (2020) 109–119, https://doi.org/10.1016/j.nanoms.2019.09.003.
[16] P.-C. Kang, Y.-S. Ou, G.-L. Li, J.-K. Chang, C.-Y. Wang, Room-temperature hydrogen adsorption via spillover in Pt nanoparticle-decorated UiO-66 nanoparticles: implications for hydrogen storage, ACS Appl. Nano Mater. 4 (2021) 11269–11280, https://doi.org/10.1021/acsanm.1c02862.
[17] H. Zhou, J. Zhang, J. Zhang, X. Yan, X. Shen, A. Yuan, High-capacity room-temperature hydrogen storage of zeolitic imidazolate framework/graphene oxide promoted by platinum metal catalyst, Int. J. Hydrog. Energy 40 (2015) 12275–12285, https://doi.org/10.1016/j.ijhydene.2015.05.199.
[18] L. Wang, N.R. Stuckert, H. Chen, R.T. Yang, Effects of Pt particle size on hydrogen storage on Pt-doped Metal−Organic framework IRMOF-8, J. Phys. Chemi. C 115 (2011) 4793–4799, https://doi.org/10.1021/jp111800c.
[19] M. Choi, S. Yook, H. Kim, Hydrogen spillover in encapsulated metal catalysts: new opportunities for designing advanced hydroprocessing catalysts, ChemCatChem 7 (2015) 1048–1057, https://doi.org/10.1002/cctc.201500032.
[20] Laleh Farzaneh, Nakhaei Pour Ali, A DFT Study of Hydrogen Adsorption on Metallic Platinum: Associative or Dissociative Adsorption, PREPRINT (Version 1) Available at Research Square, 2022.
[21] S.U.B. Ramakrishna, D. Srinivasulu Reddy, S. Shiva Kumar, V. Himabindu, Nitrogen doped CNTs supported Palladium electrocatalyst for hydrogen evolution reaction in PEM water electrolyser, Int. J. Hydrog. Energy 41 (2016) 20447–20454, https://doi.org/10.1016/j.ijhydene.2016.08.195.
[22] S. Martin, P.L. Garcia-Ybarra, J.L. Castillo, Ten-fold reduction from the state-of-the-art platinum loading of electrodes prepared by electrospraying for high temperature proton exchange membrane fuel cells, Electrochem. Commun. 93 (2018) 57–61, https://doi.org/10.1016/j.elecom.2018.06.007.
[23] Z. Wei, H. Wang, C. Zhang, K. Xu, X. Lu, T. Lu, Reversed charge transfer and Enhanced hydrogen spillover in platinum Nanoclusters Anchored on Titanium oxide with Rich oxygen Vacancies Boost hydrogen evolution reaction, Angew. Chem. 133 (2021) 16758–16763, https://doi.org/10.1002/ange.202104856.
[24] A. Alinezhad, L. Gloag, T.M. Benedetti, S. Cheong, R.F. Webster, M. Roelsgaard, B. B. Iversen, W. Schuhmann, J.J. Gooding, R.D. Tilley, Direct Growth of highly strained Pt Islands on Branched Ni nanoparticles for improved hydrogen evolution reaction activity, J. Am. Chem. Soc. 141 (2019) 16202–16207, https://doi.org/10.1021/jacs.9b07659.
[25] B. Qiao, J. Liu, Y.-G. Wang, Q. Lin, X. Liu, A. Wang, J. Li, T. Zhang, J. (Jimmy) Liu, Highly efficient catalysis of preferential oxidation of CO in H $_2$ -Rich stream by gold

single-atom catalysts, ACS Catal. 5 (2015) 6249–6254, https://doi.org/10.1021/acscatal.5b01114.
[26] L. Bai, X. Wang, Q. Chen, Y. Ye, H. Zheng, J. Guo, Y. Yin, C. Gao, Explaining the size dependence in platinum-nanoparticle-catalyzed hydrogenation reactions, Angew. Chem. Int. Ed. 55 (2016) 15656–15661, https://doi.org/10.1002/anie.201609663.
[27] R.J. Isaifan, S. Ntais, E.A. Baranova, Particle size effect on catalytic activity of carbon-supported Pt nanoparticles for complete ethylene oxidation, Appl. Catal. Gen. 464–465 (2013) 87–94, https://doi.org/10.1016/j.apcata.2013.05.027.
[28] D. Yan, J. Chen, H. Jia, Temperature-induced structure reconstruction to prepare a thermally stable single-atom platinum catalyst, Angew. Chem. Int. Ed. 59 (2020) 13562–13567, https://doi.org/10.1002/anie.202004929.
[29] C. Tsounis, B. Subhash, P.V. Kumar, N.M. Bedford, Y. Zhao, J. Shenoy, Z. Ma, D. Zhang, C.Y. Toe, S. Cheong, R.D. Tilley, X. Lu, L. Dai, Z. Han, R. Amal, Pt single atom electrocatalysts at graphene edges for efficient alkaline hydrogen evolution, Adv. Funct. Mater. 32 (2022) 2203067, https://doi.org/10.1002/adfm.202203067.
[30] P. van Helden, I.M. Ciobîcă, R.L.J. Coetzer, The size-dependent site composition of FCC cobalt nanocrystals, Catal. Today 261 (2016) 48–59, https://doi.org/10.1016/j.cattod.2015.07.052.
[31] R. Van Hardeveld, F. Hartog, The statistics of surface atoms and surface sites on metal crystals, Surf. Sci. 15 (1969) 189–230, https://doi.org/10.1016/0039-6028(69)90148-4.
[32] M.A. Fortunato, D. Aubert, C. Capdeillayre, C. Daniel, A. Hadjar, A. Princivalle, C. Guizard, P. Vernoux, Dispersion measurement of platinum supported on Yttria-Stabilised Zirconia by pulse H2 chemisorption, Appl. Catal. Gen. 403 (2011) 18–24, https://doi.org/10.1016/j.apcata.2011.06.005.
[33] K. Christmann, G. Ertl, T. Pignet, Adsorption of hydrogen on a Pt(111) surface, Surf. Sci. 54 (1976) 365–392, https://doi.org/10.1016/0039-6028(76)90232-6.
[34] G. Bergeret, P. Gallezot, Particle size and dispersion measurements, in: Handbook of Heterogeneous Catalysis, 2008, pp. 738–765.
[35] TPD-info, (n.d.). http://www.zeta-pa.de/pics/ZetA-tpd-info_e.pdf (accessed April 5, 2023).
[36] J. Miller, A fundamental study of platinum tetraammine impregnation of silica2. The effect of method of preparation, loading, and calcination temperature on (reduced) particle size, J. Catal. 225 (2004) 203–212, https://doi.org/10.1016/j.jcat.2004.04.007.
[37] M. Smiljanić, S. Panić, M. Bele, F. Ruiz-Zepeda, L. Pavko, L. Gašparič, A. Kokalj, M. Gaberšček, N. Hodnik, Improving the HER activity and stability of Pt nanoparticles by Titanium Oxynitride support, ACS Catal. 12 (2022) 13021–13033, https://doi.org/10.1021/acscatal.2c03214.
[38] D. Liu, X. Li, S. Chen, H. Yan, C. Wang, C. Wu, Y.A. Haleem, S. Duan, J. Lu, B. Ge, P. M. Ajayan, Y. Luo, J. Jiang, L. Song, Atomically dispersed platinum supported on curved carbon supports for efficient electrocatalytic hydrogen evolution, Nat. Energy 4 (2019) 512–518, https://doi.org/10.1038/s41560-019-0402-6.
[39] A. Bjelajac, D. Kopač, A. Fecant, E. Tavernier, R. Petrović, B. Likozar, D. Janaćković, Micro-kinetic modelling of photocatalytic CO_2 reduction over undoped and N-doped TiO_2, Catal. Sci. Technol. 10 (2020) 1688–1698, https://doi.org/10.1039/C9CY02443C.